Long-term conduction behavior of white-light emitting ZnS-based phosphor films

Yun-Hi Lee,[a] Young-Sik Kim, Byeong-Kwon Ju, Man-Young Sung,[b] and Myung-Hwan Oh
Korea Institute of Science and Technology, P.O. Box 131, Seoul, Korea

(Received 23 September 1998; accepted for publication 29 March 1999)

To investigate systematically the causes of the aging of thin film electroluminescent devices, time-dependent current–voltage characteristics of doubly doped ZnS:Pr, Ce, Mn layer has been investigated under a direct current high field as one of the accelerated aging methods. The surface roughness along to the direction perpendicular to the indium-tin-oxide–glass substrate and the high peak-to-valley roughness are assumed to be the main sources for current fluctuations during the measurement. It was observed that the leakage current level after long-term stressing increased or decreased depending on post-treatment indicating that the bulk-controlled conduction was the dominant mechanism determining long-term behavior and this mechanism is not sensitive to the variations in the deposition parameters. The experimental results indicate the fact that the long-term conduction behavior of ZnS-based film may be related to defect redistribution after lowering barrier height during initial stressing. Finally, we suggest that an enhancement of contact adhesions via surface smoothing of the upper interface can contribute to the long-term stability. © *1999 American Institute of Physics.* [S0021-8979(99)05713-8]

I. INTRODUCTION

There has been interest in the potential use of high quality phosphor, such as ZnS, for various applications which include color thin film electroluminescent devices (TFELD), field emission display (FED), and cathode ray tube (CRT) applications.[1] Study on the transport properties and the electrical conduction mechanism in ZnS-based phosphor is extremely important in understanding and developing full-color devices by using white. In view of the luminescence excited by hot electrons accelerated by high field over 1 MV/cm, the emphasis of studies has focused upon the evaluation method of degradation behavior of ZnS via generation of residual gas during vacuum operation[2] or shift of turn-on voltage of luminance.[3–5] In TFEL applications, Mikami *et al.*[6] suggest that aging progressed depending on two types of conduction limiting processes by taking into account that the high-field conduction inside the ZnS layer appears at an electric field strength comparable to the field ranges required for electron tunneling from the insulator-phosphor interfaces. One is the bulk-limited current[7] where the transferred charge is determined by the high-field conductivity of the ZnS layer and the other is the carrier transport characteristics limited by the probability of tunnel injection from the insulator-phosphor interfaces.

Recently, high-field direct current (dc) conduction in undoped epitaxial ZnS films were reported and compared to that from sputtered ZnS.[8] According to the report, the appearance of a significant current fluctuation hindered a further systematic study on the conduction mechanism, but this large current fluctuations again support a bulk-controlled conduction mechanism.[9–11]

For more understanding on the conduction mechanism in doped-ZnS films, a study on the time-dependent behavior of the electrical conduction of the trivalent-doped ZnS film would be required, however, it has not been a subject to study thus far. In this article, we present the time-dependent current–voltage characteristics of ZnS:Pr, Ce, Mn layers prepared with various post-deposition treatments.

II. EXPERIMENTS

In this work indium tin oxide (ITO)–ZnS:Pr, Ce, Mn–Al capacitors have been studied for leakage current and time-dependent behavior. The 450–550 nm thick ZnS:Pr (0.3 mol %), Ce (0.3 mol %), and Mn (0.002 mol %) films were formed by Edwards electron-beam evaporator (E306A) equipped with TELEMARK high power *E*-gun. During the deposition vacuum pressure was about 2×10^{-6} Torr. The phosphor films on ITO-coated Corning 7059 glass (1.1 mm thick) substrate were crystallized by a conventional vacuum annealing at 400 °C for 30 min (sample No. 1) and 60 min (No. 2). Some part of No. 1 films underwent an additional treatment such as an additional annealing in oxygen atmosphere for 10 min (No. 3). For the oxygen plasma treatment, the specimens were exposed to oxygen plasma gases in reactive ion etcher for 5 min (No. 4).

The roughness parameters and the chemical composition of the topmost surface of the films were obtained by the atomic force microscopy and the Auger electron spectroscopy (AES), respectively. Direct current–voltage ($I-V$) characteristics for M(ITO)–I(ZnS:Pr,Ce)–M(Al) structure were measured using a fully automated Keithley 237 dc high voltage source and a measuring unit. The capacitance and the

[a]Electronic mail: lyh@kistmail.kist.re.kr
[b]Also at Korea University, Seoul, Korea.

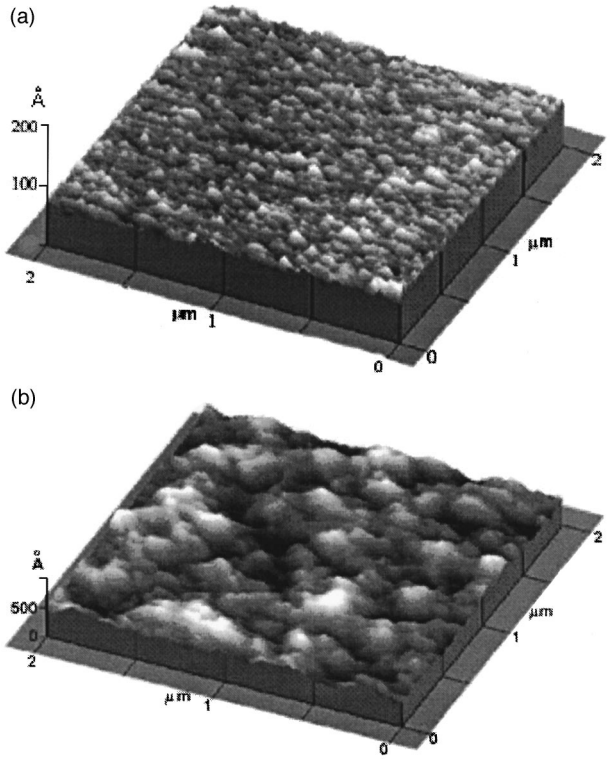

FIG. 1. The observed roughness images for (a) No. 1 and (b) No. 2.

loss tangent characteristics as a function of dc bias and frequency were obtained using the Hewlett–Packard 4192A impedance analyzer.

III. RESULTS AND DISCUSSION

A. Variation of surface roughness with a post-deposition anneal

To study the influence of post-deposition annealing on the surface morphology,[5–12] an important parameter determining the electron injection properties of TFEL, the surface roughness of the ZnS:Pr,Ce films was examined using the atomic force microscope (AFM). Figure 1(b) and Fig. 2(c) indicate that the surface roughness for the sample No. 2 and O_2 plasma treated film (No. 4) is greater than that for that of No. 1 as shown in Fig. 1(a). While the surfaces of No. 1 and No. 3 were sufficiently smooth for TFEL application as summarized in Table I, the surface roughness of the ZnS increased with increasing annealing time (No. 2) and O_2 plasma treatment (No. 4), because of the efficient columnar formation in No. 2 after long annealing and the slightly etched surface in No. 4. The surface roughness parallel to the ITO–glass substrate and the high peak-to-valley roughness in No. 2 film are assumed to be the main sources for the current fluctuations during the measurement.

B. Initial current–voltage characteristics for both polarities

The time-zero leakage current versus voltage measurement was made on No. 1 (anneal for 30 min), No. 2 (anneal for 60 min), and No. 3 (No. 1+an additional anneal) capacitors after initial burn-in. At the first ramp, the dc leakage

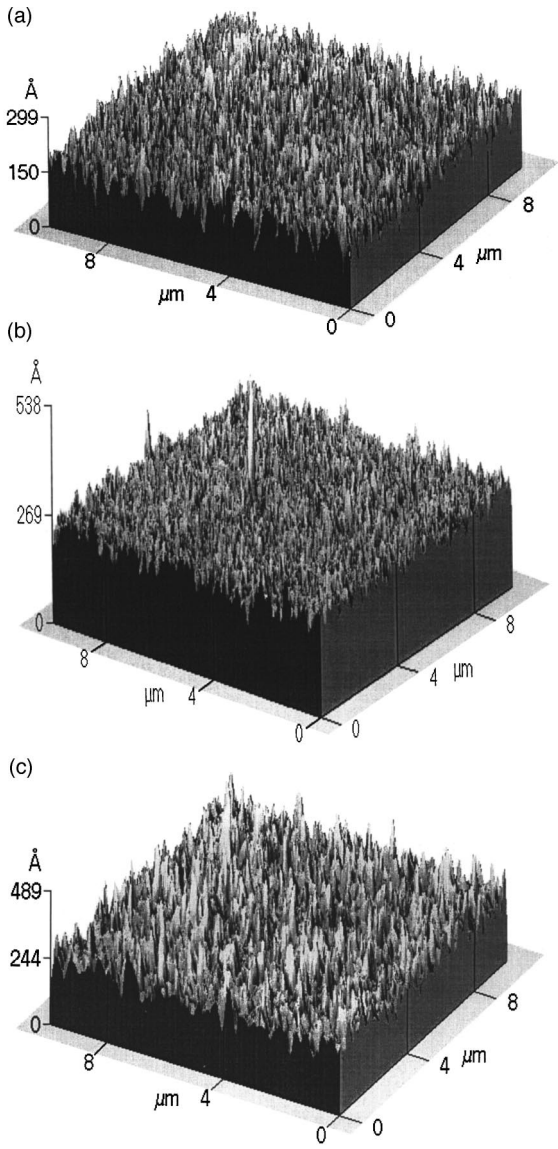

FIG. 2. The observed roughness images for (a) No. 1, (b) No. 3, and (c) No. 4.

current density increased approximately linearly with voltage at very low fields, i.e., the leakage current is initially carried by thermally excited carriers contained in the ZnS layer, which has ohmic characteristics for both polarities. At a higher field region shown in a semilog plot of Fig. 3 for Al(−), the linear current–voltage behavior indicates the Schottky-type emission and the slope yields the dynamic dielectric constant, i.e., optical refractive index of the ZnS film.[13] Since both types of capacitors show slightly different slopes, we can assume that the potential barriers at Al–ZnS as seen from the Al (interface barrier height, Φ_b) were different from each other. When carrying out multiple ramping up to 60%–80% of the breakdown voltage, a decrease in the field-dependent leakage was observed. The voltage-dependent current reached its lowest level, after multiple voltage ramping, e.g., 3–5 voltage sweeps. After the first measurement on a fresh device, the subsequent $I-V$ curves showed diminished leakage levels. This indicates that during

TABLE I. Roughness parameters estimated from AFM images for the Nos. 1, 2, 3, and 4.

	Scan area (μm^2)	Peak-to-valley roughness (nm)	Root-mean-square roughness (nm)	Average roughness (nm)
No. 1	10×10	3.0	3.3	2.6
(annealing for 30 min)	3×3	3.2 (max.: 4.1)	3.8	2.3
No. 2	10×10	26.5	12.1	6.1
(annealing for 60 min)	3×3	6.9	6.1	4.9
No. 3	10×10	2.9	2.5	2.0
(No. 1+anneal in O_2 for 10 min)	3×3	2.2	2.8	2.2
No. 4	10×10	4.4	4.2	3.2
(No. 1+O_2 plasma exposure for 10 min)	3×3	4.7	5.1	3.9

the measurement there is a rearrangement of surface space charges (perhaps ionic), which then alter the equilibrium Fermi level within the film.

Figure 3 indicates that the current at the negative bias region (Al−) is much higher than the current at the positive bias region. Especially, the extra annealing step for No. 2 is understood to be the cause for the significant asymmetry and the difference in current levels, depending on polarity. From this, we can assume that the potential barriers at Al–ZnS as seen from ZnS (built in potential V_b) and from the Al (interface barrier height, Φ_b) were different from each other. We confirmed that the reverse current tends to increase with further increase of the stressing time. The increase of reverse current might be caused by the generation of a high amount of sulfur vacancies at the top Al–ZnS interface than at the bottom ITO–ZnS interface. It is considered that the sulfur vacancies act as donors,[9] as follows:

$$S_s = V_s'' + 2e^- + 1/2S_2,$$

where S_s is the sulfur ion at the sulfur site, V_s'' is the ionized sulfur vacancy, and e is the electron. It is well known that the luminance (L)-applied voltage (V) characteristics are almost restored to the original ones when the degraded ZnS are annealed in H_2S atmosphere. This fact predicts that at the Al–ZnS interfaces there exists high density of sulfur vacancies or Zn excess. These sulfur deficient layers imply a large built-in fields within the ZnS. It was evident from $C-V$ results that the values of the dielectric constant increased with increasing S (or O) ratio to Zn. This may be due to the fact that substitution of O at the sulfur sites increases the unit cell size and hence polarization is enhanced. At much higher voltages, the mechanism is not clear but is thought to be intertrap tunneling and/or impact ionization of impurities and crystal lattice.

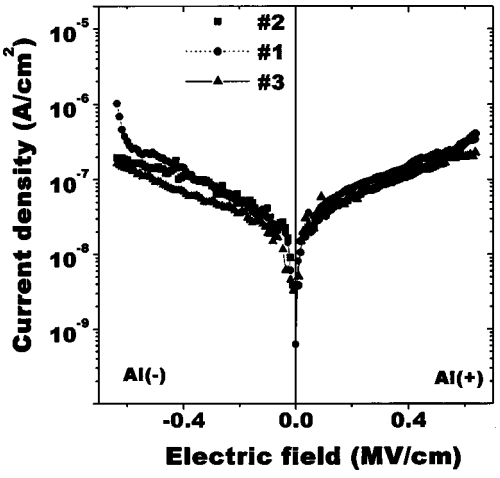

FIG. 3. DC current–voltage characteristics of ZnS capacitors.

The leakage current of metalorganic chemical vapor deposition (MOCVD)-prepared ZnS:Mn at high temperatures and high field is frequently referred to as the Poole–Frenkel (PF) conduction[6,7] and the depth of the trapping center for the conduction is about 0.3–0.1 eV, independent of the growth methods, conditions, and the luminescent centers. The conductivity does not depend on the trap depth but on the trap density.[7] On the other hand, current–voltage characteristics for e-beam evaporated ZnS:Mn showed space-charge-limited conduction showing V^n ($n \sim 1-2$) with slight thickness dependence.

The ohmic nature of the ITO–ZnS interface in the full range implies that the surfaces of the ZnS in contact with ITO are different from those on Al side at this work. Probably, there is a difference in the nature of the chemical bonding between the ZnS and ITO compared to bonding between the ZnS and Al; Al does not produce a strong chemical bond with the ZnS, while In(Sn) and oxygen ions in the ITO interact with sulfur ion and Zn in the ZnS, thus forming a chemical bond. In the sulfur states, the dangling bonds can be present even after the post-deposition annealing regardless of the process time and conditions. However, in the ITO–ZnS case, most of the dangle bonds disappear due to the chemical interaction with ITO.

At the initial stressing stage, Fig. 4 shows log(J) vs ($E^{1/2}$) curves to reveal the $J-V$ behavior subject to electrode-limited Schottky conduction for Al(−). The arrows in Fig. 4 indicate the points of an approximate onset of the linear behavior on each curve. Unlike the curves in Figs. 4(a) and 4(b) for No. 1 and No. 3, the curves for No. 2 show that the onset voltage of the linear behavior is increased as the temperature is elevated. This indicates that at high temperatures the leakage current of type No. 2 capacitors is dominated by a more complex mechanism. Considering the fact that the conduction due to the Schottky emission depends on the work function of the contact metal, the barrier lowering

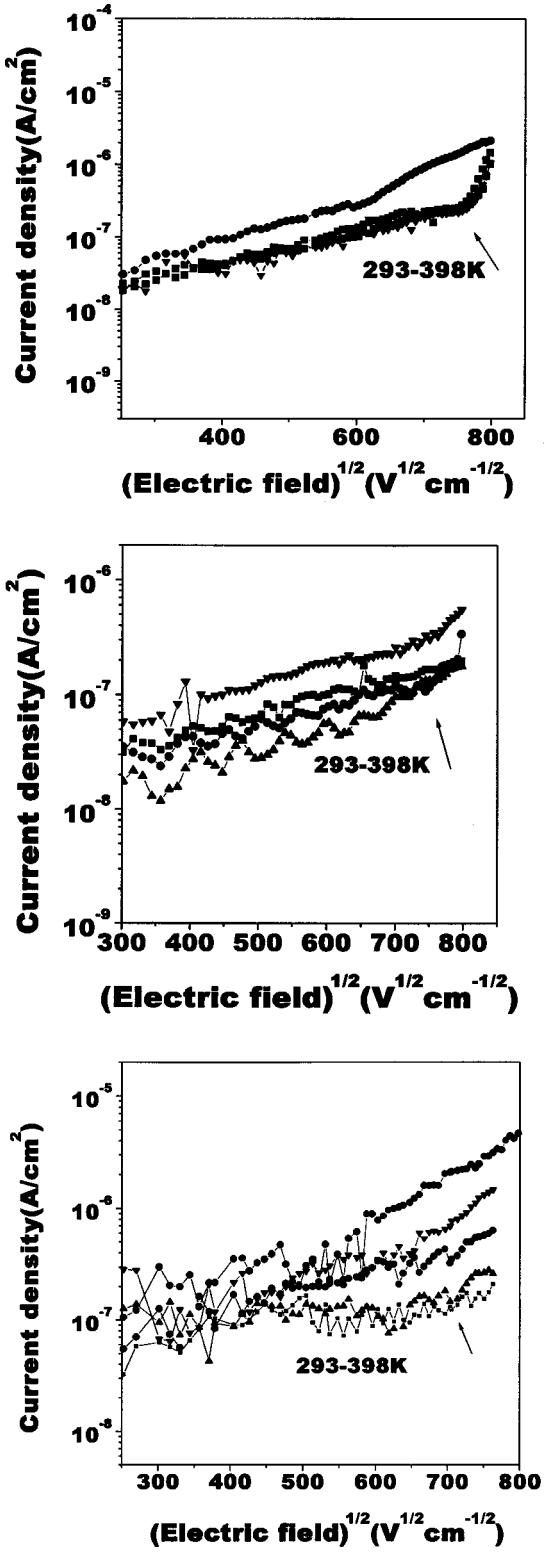

FIG. 4. Temperature dependence of leakage current for Nos. 1, 2, and 3 as a function of square root of the applied voltage in 26–35 V range. Leakage current were measured when temperatures were increased from 25 to 120 °C.

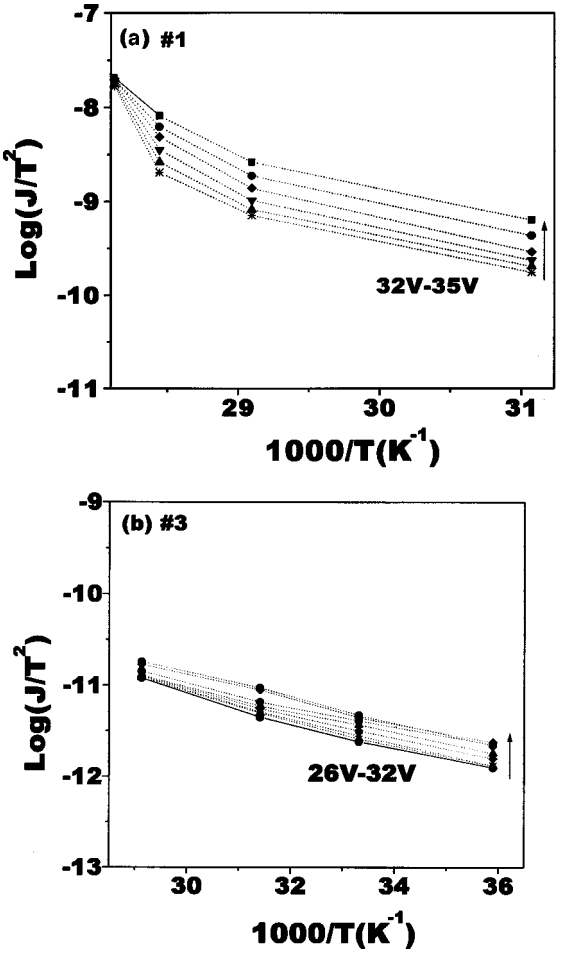

FIG. 5. Variations of $\log(J/T^2)$ with $1000/T$ of the films. The measured values are over the range from 32 to 35 and 26 to 32 V for No. 1 and No. 3, respectively.

by image force, and the surface states, we can tentatively conclude that the upper side (Al) of No. 2 films contains higher concentration of the surface or the interface defects than No. 1. Here, we suggest that the high surface roughness is one of the factors for the increase of surface defects, as well as the strongly temperature-dependent current.

C. Effect of the post-process on the activation energy

To study the influence of the doping material on the conduction behavior ZnS:Pr, Ce, Mn films were fabricated and temperature dependence of leakage current were measured. If the current obeys the Schottky emission model, the fitted curves in the semilog plot (J/T^2) vs $1000/T$ should be straight. Figure 5 shows the variation of $\log(J/T^2)$ as a function of $1000/T$ in the 26–35 V range at various measuring temperatures. The plot for No. 1 shows deviation from linearity, suggesting maintenance of electrode-limited conduction. Figure 6 shows the Arrhenius plots of the leakage current. Their activation energy calculated from the slopes of $\log(J)$ vs $1000/T$ plot[13] were about 0.21 (ITO−) and 0.34 eV(Al−) for No. 3 and 0.22 (ITO−) and 0.15 (Al−) for No. 1. On the other hand, a negative energy (ITO−) and 0.13 eV(Al−) for No. 2 were obtained. The behavior under the negative bias on Al is shown in Fig. 6(b). The leakage current density decreased with temperature. A similar effect observed in the ferroelectric ceramic[10,11] has been closely related to the acceptor-doped grain boundaries with donor-doped grains[14,15] and originates from an increase in the

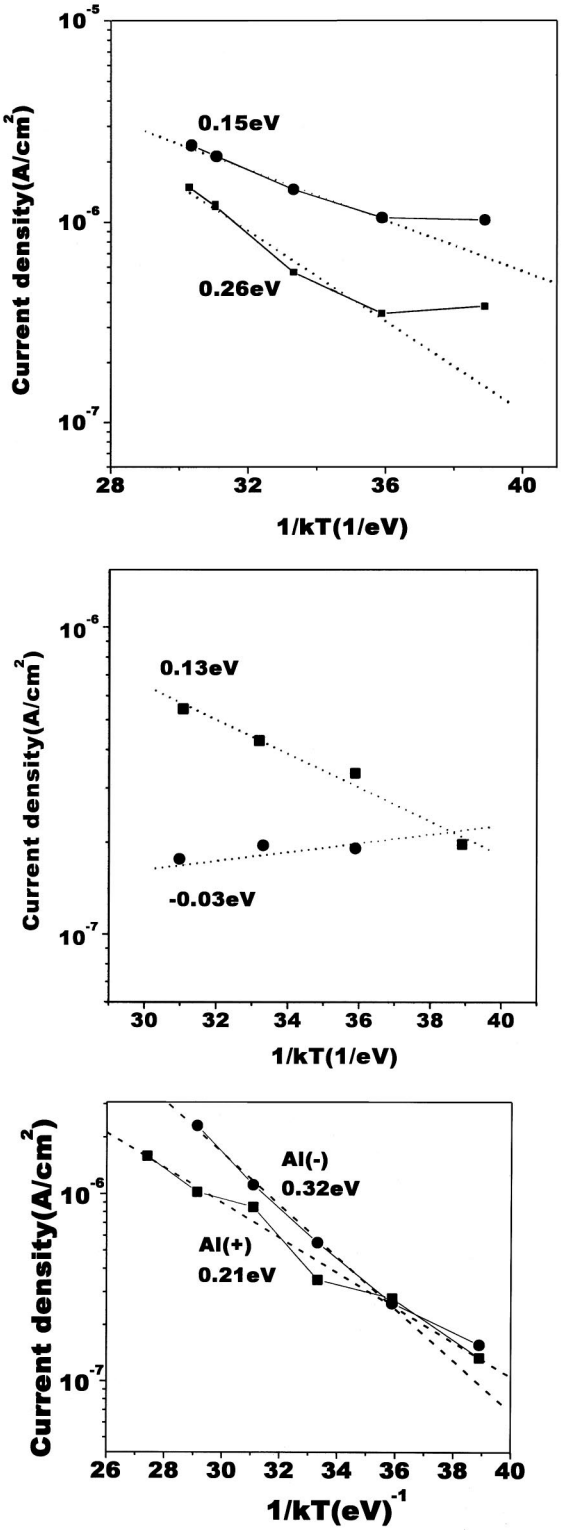

FIG. 6. Arrhenius plots of the leakage current at 35 V of 550 nm thick Nos. 1, 2, and 3 films.

height of the grain-boundary potential barrier with a rapid drop of the dielectric constant with temperature.[16,17]

D. Time-dependent leakage current behavior

As generally suggested for the insulating films, it is important to investigate the time dependence of the current under the constant voltage stress before drawing any conduction mechanism.[18,19] In our work, under the application of a constant field, the leakage current density through the films was monitored as a function of time as shown in Fig. 7 and Fig. 8. Figure 7 shows the time-dependent behavior of the leakage current during the stressing with 0.6 MV/cm for over 4000 s. Samples No. 1 and No. 3 showed a stable current level after a stress time of 0.6 h. For No. 2, a rapid increase in the current level was observed accompanied with strong fluctuation after 0.6 h of stressing. These plots indicate that the midterm behavior of the leakage current under a high-field stress depends on both the annealing conditions and the post-treatment even if the initial leakage currents are nearly the same level as shown in Fig. 8. Note that a dielectric breakdown was occurred at No. 1 and No. 2 after stressing about 2 h and this effect appeared at a reduced current level, as shown in Fig. 9, via decrease of the effective electrode area by blowing up Al electrode.

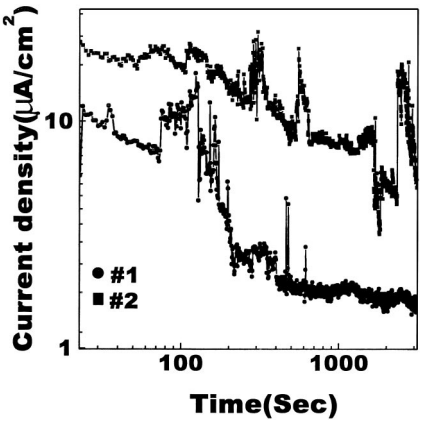

FIG. 7. Leakage current–time characteristics for ZnS:Pr, Ce, Mn, F, Cl films under stressing at 0.67 MV/cm.

On the other hand, the long-term current seems to obey a power law which is essentially a nearly linear dependence of $\log(J)$ on $\log(t)$. This may be attributed to either the trapping of charge carriers or the space-charge relaxation in our films as observed in SiO_2.[20]

E. Conduction behavior of the aged phosphor film

After long-term stressing with 0.6 MV/cm field for 2 h at 423 K, the current–voltage curve obtained from these aged specimens at 298 K is significantly different from those in Fig. 2, as illustrated in Fig. 9. The current is linearly dependent on voltage (ohmic) for small voltages: $J=qn_0\mu V/d$, where q is the electronic charge, n_0 is the equilibrium carrier concentration, μ is the carrier mobility, and d is the ZnS thickness. On the other hand, at high voltages, J for Nos. 1 and 2 is expected to follow a square-law dependence on voltage: $J\sim\varepsilon\mu(V^2/d^3)$; in this regime, the injected carrier concentration exceeds the equilibrium carrier concentration in the ZnS. Thus, the increase of leakage current in No. 1 and No. 2 suggests that the lowering of the interface barrier height is resulted from the constant stress while there is no change in current density for No. 3. As a result of barrier lowering at the electrode interface, the space-charge-limited

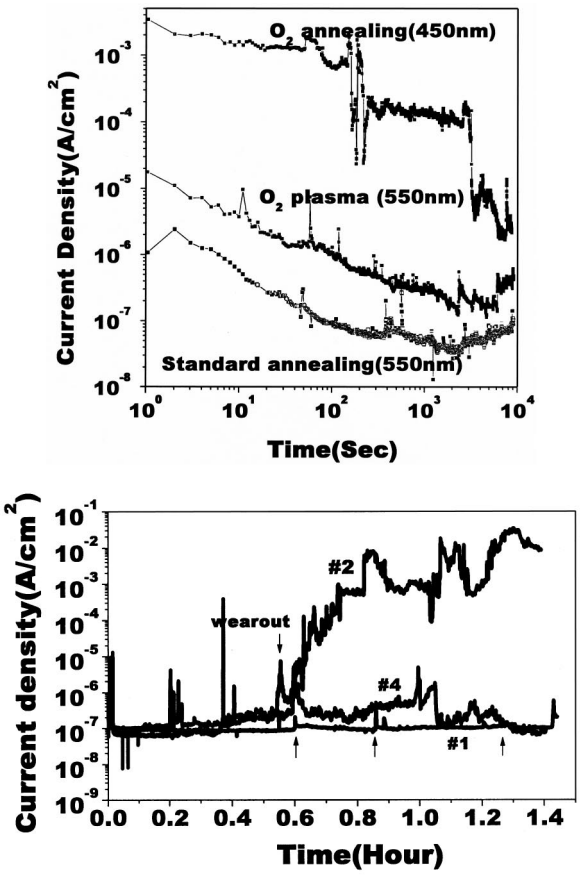

FIG. 8. Leakage current–time characteristics for ZnS:Pr, Ce, Mn, F, Cl films under stressing at 1.1 MV/cm at 293 K. The curves are observed under stressing of 1.1 MV/cm. The arrow indicates the localized electric breakdown during the stressing.

conduction appears to be dominant at high-field regime. Figure 9 can be explained as follows. There are several models describing the phenomena of time-dependent dielectric breakdown. The grain-boundary barrier-height reduction model assumes that the positively charges sulfur vacancies with a relatively high mobility electromigrate towards the cathode under dc field. Especially, when the temperature is elevated to 393 K during the high-field operation, the existing ionized sulfur vacancies within the bulk are thermally activated and begin to migrate toward the cathode under the high electric field. Finally, the sulfur vacancies accumulate near the cathode. At the anode, an electrode reaction leads to the generation of sulfur gas and electrons, leaving sulfur vacancies behind. The net result is that the space charge accumulation at the grain boundary gives rise to an increase of the leakage current and finally results in a dielectric breakdown as shown in Fig. 8. Since the interface barrier originates from the built-in potential primarily formed between the accumulated charge at the interface and the ionized sulfur vacancies near the interface, the barrier height is lowered due to the accumulation of the sulfur vacancies at the cathode. The increase of the leakage current at the low-field regime after stressing field with 0.6 MV/cm for the No. 1 and No. 2 is based on a similar mechanism. Therefore, the conduction process was changed from the interface-controlled Schottky emission as a result of barrier lowering due to the applied field and the image force to the bulk-related space-charge-limited process associated with the field enhanced thermal excitation of charge carriers from traps. If the film can withstand high field, the trap-free space-charge-limited current will eventually dominate as the time elapses. Although we did not confirm the essential nature of traps, the traps responsible for the transition would be the cooperation of the sulfur vacancies with the light emission center.

From the observed results, we can conclude that the best way to improve the time-dependent characteristics is to reduce the concentration of sulfur vacancies in the ZnS bulk, however, the long-term conduction behavior of the ZnS-based film can be controlled by the post-deposition treatment even in the case of the off-stoichiometric film.

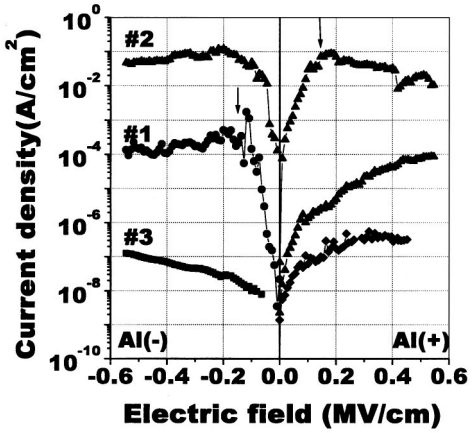

FIG. 9. Leakage current–time characteristics for ZnS:Pr, Ce, Mn, F, Cl after long-term stressing at 35 V. The arrow indicates the decrease of effective electrode area due to blowing up Al electrode via electric breakdown.

IV. CONCLUSION

The surface roughness of ZnS:Pr, Ce phosphor films parallel to the glass substrate and the high peak-to-valley resulting from hillock formation in the 60 min annealed film were assumed to be the main sources of difference at initial $I-V$ characteristics and the fluctuations with time. When carrying out multiple ramping up to 60%–80% of the breakdown voltage, the voltage-dependent current reached its lowest value. Here, the first insight of the irreversible space-charge motion in the film was obtained from the time-dependent $I-V$ measurement. This indicates that during the measurement there is a rearrangement of space charge that may be ionic. In the long-term operation, the conduction process for Al–ZnS interface was changed from the interface-controlled Schottky type to the bulk-related space-charge-limited type probably due to the trap redistribution across the ZnS:Pr, Ce phosphor film.

ACKNOWLEDGMENT

The authors would like to thank Dr. Dong-Ho Kim at Yeungnam University for reading the whole manuscript and useful comments throughout this and many other manuscripts.

[1] Y. W. Jin, J. E. Jing, J. E. Jung, Y. S. Ro, Y. J. Park, S. N. Cho, and J. M. Kim, *SID 98 Digest*, 1998, pp. 612–615.
[2] P. H. Holloway, T. A. Trottier, J. Sebastian, S. Jones, X.-M. Zhang, J.-S. Bag, B. Abrams, W. J. Thomas, and T.-J. Kim, *The 3rd International Conference on the Science and Technology of Display Phosphor*, Extended Abstract, 1997, p. 7.
[3] T. Inoguchi, M. Takeda, Y. Kahihara, Y. Nakata, and M. Yoshida, *SID 74 Digest*, 1974, p. 84.
[4] J. Watanabe, M. Wakitani, S. Sato, and S. Miura, *SID 74 Digest*, 1974, p. 288.
[5] P. M. Alt, D. B. Dove, and W. E. Howard, J. Appl. Phys. **53**, 5186 (1982).
[6] A. Mikami, K. Terada, K. Okabayashi, K. Takana, M. Yoshida, and S. Nakajima, J. Appl. Phys. **72**, 773 (1992).
[7] K. Hirabayashi, T. Shibaya, and H. Kozawagucji, IEEE Trans. Electron Devices **ED-36**, 1943 (1989).
[8] E. Bringuier and O. Briot, Appl. Phys. Lett. **67**, 3486 (1995).
[9] E. Bringuier, Philos. Mag. B **75**, 209 (1997).
[10] M. Beale, Philos. Mag. B **68**, 573 (1993).
[11] A. J. Simons and C. B. Thomas, Philos. Mag. B **68**, 465 (1993).
[12] Y. H. Lee, Y. S. Kim, B. K. Ju, and M. H. Oh, IEEE Trans. Electron Devices **ED-46**, 892 (1999).
[13] S. Ezhilvalalan and T. Y. Tseng, J. Appl. Phys. **83**, 4797 (1998).
[14] C. H. Hang *et al.*, J. Appl. Phys. **83**, 3703 (1998).
[15] W. Heywang, Solid-State Electron. **3**, 5 (1961).
[16] W. Heywang, J. Am. Ceram. Soc. **47**, 484 (1964).
[17] B. Huybrecht, K. Ishizaki, and M. Takata, J. Mater. Sci. **30**, 2463 (1995).
[18] H. Matsumoto, A. Suzuki, and T. Yabumoto, Jpn. J. Appl. Phys., Part 1 **19**, 71 (1980).
[19] K. Watanabem, A. J. Hartmann, R. N. Lamb, and J. F. Scott, J. Appl. Phys. **84**, 2170 (1998).
[20] C. Sudhama, A. C. Campbell, P. D. Maniar, R. E. Jones, R. Moaaaami, C. J. Mogab, and J. C. Lee, J. Appl. Phys. **75**, 1014 (1998).